

Nucleation and growth of second phase precipitates under non-isothermal conditions *

A. R. Massih^{1,2} and L. O. Jernkvist¹

¹ *Quantum Technologies, Uppsala Science Park, SE 751 83 Uppsala, Sweden and*

² *Materials Science, Malmö University, SE 205 06 Malmö, Sweden*

(Dated: November 21, 2018)

The Langer-Schwartz equations for precipitation are formulated to calculate nucleation, growth and coarsening of second phase precipitates under non-isothermal situations. A field-theoretic steady-state nucleation rate model is used in the analysis. The field-theoretic nucleation rate is compared with the classical nucleation rate relation derived from the Fokker-Planck equation. This integrated model is used to simulate a bcc-to-hcp phase quenching and subsequent annealing in the hcp phase of a dilute zirconium alloy, where the mean precipitate size, number density and the degree of supersaturation are calculated as a function of time. The influence of cooling rate on the aforementioned parameters is evaluated. A lower cooling rate results in larger precipitates with a smaller number density in concordance with observations.

I. INTRODUCTION

Various important properties of engineering alloys, such as their mechanical strength and toughness, creep and corrosion resistance, magnetic and superconducting behaviors, are basically governed by the presence and characteristics of second phase precipitated particles (SPPs) [1]. In many material processing methods, the SPP characteristic is controlled by quenching the material from a high temperature phase, where the constituents of the SPPs are in solid solution, to a low temperature phase, in which precipitation occurs and a distribution of SPPs is observed. This process embraces such phenomena as nucleation, spinodal decomposition, late stage growth and coarsening, which are broadly described by the framework of the kinetics of first-order transitions [2].

For example, when a binary alloy system is quenched from an equilibrium state (phase) to a non-equilibrium state inside a coexistence curve of its phase diagram, the quenched system gradually transforms from the non-equilibrium state to an equilibrium state, consisting of two coexisting phases. This transformation occurs by time-dependent spatial fluctuations of the local concentration of one of the two component species. Commonly, two different kinds of instabilities are considered; in one case the solid solution experiences a shallow quench in the metastable region, in another, it is quenched deeply into the unstable region of the miscibility gap [1]. In the former case, the instability is due to the formation of stable nuclei via localized composition fluctuations, requiring to surmount an energy barrier that is characterized by an incubation period. This corresponds to a metastable phase and the transformation is by nucleation and growth. In the latter case, the instability is caused by the formation of non-localized, small-amplitude, spatially extended composition fluctuations that grow spontaneously in amplitude as the time after the quench proceeds [3]. For a binary system, this phenomenon is called spinodal decomposition, for which the quenched state lies within the boundary between unstable and metastable states, the so-called spinodal curve.

Langer and Schwartz [4] have developed a detailed theory describing the nucleation, growth and coarsening of droplets in metastable, near-critical fluids. Wendth and Haasen [5] adapted this theory for solid solutions and used it to interpret the precipitation of γ' -Ni₃Al SPPs in Ni-14 at.%Al. Later, Kampmann and Wagner [6] introduced a non-linearized Gibbs-Thomson relation into the Langer-Schwartz equations in order to account for cases where the surface tension of precipitates and the supersaturation are large. They also included an empirical time-dependent factor on the steady-state nucleation rate to include transient nucleation kinetics that has been observed in many experiments. Kampmann and Wagner used the model to interpret and explain observations on β' -Cu₄Ti particles in Cu-1.9 at.%Ti alloy.

In the present paper, we consider homogeneous nucleation, growth and coarsening of SPPs under non-isothermal conditions. The Langer-Schwartz equations for the precipitation kinetics are formulated in a way that can be used to calculate nucleation and growth of SPPs under time-varying temperature situations such as quenching. A field-theoretic steady-state nucleation rate model is used in our evaluation. Moreover, the basic models for growth and coarsening are presented, followed by a computation of an isothermal experiment on a copper-cobalt alloy phase transformation, and a simulation of a body-centered cubic (bcc) to hexagonal close-packed (hcp) phase quenching and subsequent annealing in the hcp phase of a dilute zirconium alloy.

* This is an expanded version of the paper presented in the International Conference on Solid-Solid Phase Transformation in Inorganic Materials 2005 (PTM 2005), May 29 - June 3, 2005, Phoenix, Arizona, USA.

II. MODELS

The models considered here describe the phenomena of homogeneous nucleation, growth and coarsening of second phase precipitates in non-isothermal conditions in an integrated fashion. The precipitates are assumed to be spherical and at each instant are in local equilibrium with their surrounding; therefore the concentration near the SPP/matrix interface is determined by the Gibbs-Thomson boundary condition. A key variable defining the state of the system is the supersaturation; here defined as $x \equiv \ln(C/C_\infty)$, where C is the solute concentration in the matrix, which is time-dependent, and C_∞ the solubility limit or the equilibrium solute concentration, which is strongly temperature dependent. The Langer-Schwartz theory of precipitation basically comprises a nucleation model and a growth model. In this section we outline these models and describe our formulation of the theory for non-isothermal applications.

A. Nucleation

1. Classical Theory

Consider that a spherical (or circular) particle with radius R is emerged from a metastable state. The particle free energy consists of the surface and the bulk energy parts,

$$F(R) = S_d \left(\sigma R^{d-1} - \frac{\mu_e}{d} R^d \right), \quad (1)$$

where d is the spatial dimensionality, $S_3 = 4\pi$ and $S_2 = 2\pi$, σ the surface energy, and μ_e the difference in free energy density (per unit volume) between the metastable and stable phases. The function $F(R)$ goes through a maximum at a critical radius $R = R_c = (d-1)\sigma/\mu_e$. The height of the nucleation energy barrier is given by:

$$F_c = F(R_c) = \frac{S_d}{d} \sigma R_c^{d-1}. \quad (2)$$

The probability of formation of a particle of radius R is $P \sim \exp[-\beta F(R)]$, where $\beta = 1/k_B T$ with k_B Boltzmann's constant and T the temperature. Thus the critical nucleus, which maximizes F , is the least probable one. Once the particle forms, it will grow to reduce its free energy.

The basic ingredient of the considered model is the nucleation rate of the secondary phase precipitates. In the standard formulation, attributed to Ya. B. Zel'dovich [7], the nucleation process is described by a Fokker-Planck equation:

$$\frac{\partial n}{\partial t} = \frac{\partial}{\partial R} \left(B \frac{\partial n}{\partial R} \right) + \beta \frac{\partial}{\partial R} \left(B n \frac{\partial F}{\partial R} \right), \quad (3)$$

where $n = n(R, t)$ is the number of SPP in the radius interval $[R, R + dR]$ per unit volume at time t , $B = B(R)$ a nucleation size diffusion coefficient and F the SPP free energy. After a transient time t_0 , a constant nucleation rate of SPPs with radii larger than R_c prevails, $J = \text{const}$. More concretely, if $R \gg R_c$, $n(R, t)dR = Jdt$ is the number of growing newly emerging particles in a time interval dt per unit volume and is independent of R [8]. The steady-state solution of Eq. (3), $n = n_s(R)$ is obtained by integration, viz.,

$$n_s(R) = J e^{-\beta F(R)} \int_R^\infty dr B(r)^{-1} e^{\beta F(r)}, \quad (4)$$

where the condition $n_s(R) \rightarrow 0$ as $R \rightarrow \infty$ was imposed. Next, noting that the steady-state solution of the Fokker-Planck equation is determined by the Boltzmann distribution, i.e., $n_s = n_\ell \exp[-\beta F(R)]$, an expression for J can be obtained, when R is near R_c , giving (Appendix A)

$$J = (2\pi)^{-1/2} (d-1)^{1/2} D_n (S_d \beta \sigma)^{-1/2} R_c^{-(d+1)/2} n_\ell \exp(-\beta F_c), \quad (5)$$

where $D_n = S_d \beta \sigma R_c^{d-1} B_c$ is the critical nucleation diffusivity with $B_c = B(R_c)$. Relating the critical radius to the supersaturation x and the capillary length ℓ according to: $R_c = \ell/x$, where $\ell = 2\beta\sigma v_a$ and v_a the atomic volume of the precipitate, Eq. (5) is expressed in terms of the supersaturation, i.e.,

$$J = \sqrt{\frac{d-1}{2\pi d}} D_n n_\ell \left(\frac{x_0}{\ell} \right) \left(\frac{x}{x_0} \right)^{\frac{d+1}{2}} \exp \left[- \left(\frac{x_0}{x} \right)^{d-1} \right], \quad (6)$$

where

$$x_0 = \left(\frac{S_d \beta \sigma}{d} \right)^{\frac{1}{d-1}} \ell. \quad (7)$$

Relation (6) is the classical expression for the nucleation rate formulated in d spatial dimensions as a function of the supersaturation. The scaling in the critical region suggests that the Boltzmann prefactor is $n_\ell \sim \ell^{-(d+1)}$. Whence, setting $\mathcal{A} \equiv \sqrt{(d-1)/2\pi d}$, Eq. (6) can be written as

$$J = \mathcal{A} \frac{D_n x_0}{\ell^{d+2}} \left(\frac{x}{x_0} \right)^{\frac{d+1}{2}} \exp \left[- \left(\frac{x_0}{x} \right)^{d-1} \right]. \quad (8)$$

2. Field Theoretic Approach

The nucleation rate in the field-theoretic formulation [9] begins from the relation that links the steady-state nucleation rate with the imaginary part of the free energy

$$J = \frac{\beta \kappa}{\pi} \Im [F(\mu_e)], \quad (9)$$

where κ is a kinetic factor related to the diffusivity via $\kappa = (d-1)D_n \ell / R_c^3$. Relation (9) has been evaluated by various investigators and more carefully by Günther, Nicole and Wallace [10], which for $d = 3$ takes the form (Appendix B)

$$J = \mathcal{B} \frac{D_n x_0^6}{\ell^5} \left(\frac{x}{x_0} \right)^{2/3} \exp \left[- \left(\frac{x_0}{x} \right)^2 \right], \quad (10)$$

where $\mathcal{B} = 6^5 / (288\pi\sqrt{3})$. Equation (10) is strictly valid for low supersaturations, i.e., when $x/x_0 \ll 1$. Langer and Schwartz [4] have heuristically extended this expression for large values of x according to

$$J = \mathcal{B} \frac{D_n x_0^6}{\ell^5} \left(\frac{x}{x_0} \right)^{2/3} \left(1 + \frac{x}{x_0} \right)^{3.55} \exp \left[- \left(\frac{x_0}{x} \right)^2 \right]. \quad (11)$$

The behavior of the aforementioned models for the nucleation rate, Eqs. (8), (10) and (11) are illustrated in Fig. 1 for $d = 3$, where the scaled nucleation rate K is plotted against the scaled supersaturation x/x_0 (Eq. (8) is scaled by $\mathcal{A} D_n x_0 / \ell^{d+2}$, while Eqs. (10) and (11) are scaled by $\mathcal{B} D_n x_0^6 / \ell^5$).

B. Growth and Coarsening

1. Theory

The details of the Langer and Schwartz theory have been clearly described in their original work [4] and reviewed in a number of publications ([1], [2], [11], [12]). We only summarize its basic ingredients in order to fix notation. The basic equations of the Langer-Schwartz theory are those of the Lifshitz and Slyozov [13], supplemented by a source of droplets (spherical precipitates) which describes the nucleation event. The continuity equation for the droplet distribution function $n = n(R, t)$ is

$$\frac{\partial n}{\partial t} + \frac{\partial}{\partial R} \left[\frac{dR}{dt} n \right] = j(R), \quad (12)$$

where $j(R)$ is the distributed nucleation rate of precipitates, $J = \int_{R_c}^{\infty} j(R) dR$, and as before J stands for the nucleation rate per unit volume. Langer and Schwartz made a simplifying assumption that only precipitates with $R > R_c$ are to be counted as part of the second phase. The SPP number density N is given by $N = \int_{R_c}^{\infty} n(R) dR$ with their mean radius defined as $\bar{R} = \frac{1}{N} \int_{R_c}^{\infty} n(R) R dR$.

The growth rate of the spherical nucleus is controlled by the rate the solute atoms supplied to the precipitate/matrix interface via diffusion [13]

$$\frac{dR}{dt} = \frac{D}{R} \left(\frac{C(t) - C_R}{C_p - C_R} \right). \quad (13)$$

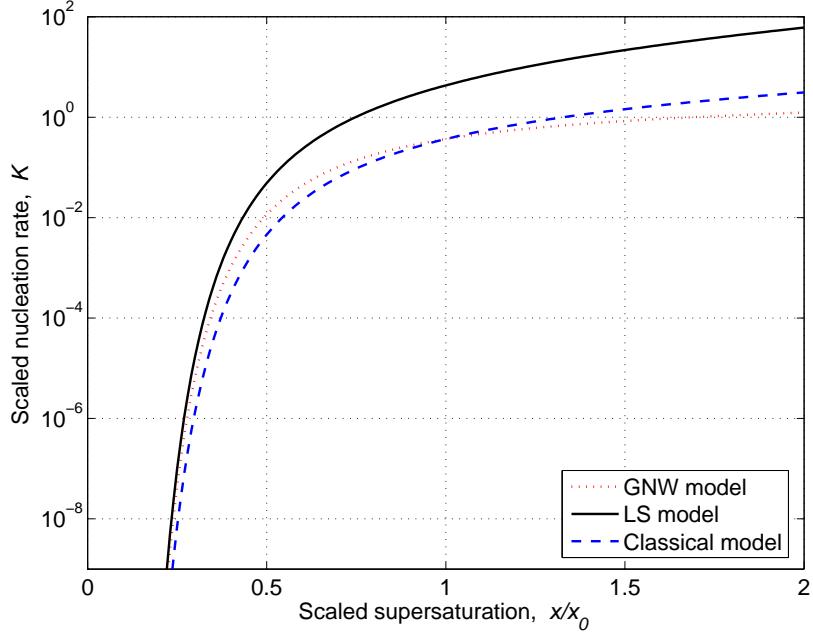


FIG. 1: The scaled nucleation rate vs. scaled supersaturation for $d = 3$, comparing predictions of Eq. (8), the classical model, Eq. (10), the GNW model, and Eq. (11), the LS model. The scaling factors used are defined in the text

Here, D is the diffusivity of the solute in the matrix, C the matrix average solute concentration, C_p the solute concentration within the precipitate, assumed to be uniform, and C_R the local solute concentration at the precipitate/matrix interface. The latter concentration is related to the solubility limit C_∞ , a temperature dependent quantity, and the curvature of the precipitate/matrix interface through the Gibbs-Thomson relation $C_R = C_\infty \exp(\ell/R)$. Also, the equation for conservation of matter must be satisfied, viz.,

$$\frac{C - C_0}{C - C_p} = \frac{4\pi\bar{R}^3}{3} N(t). \quad (14)$$

For non-isothermal conditions, where temperature is varying with time, all the temperature dependent parameters appearing in the foregoing equations must be considered and treated properly. The resulting Langer-Schwartz differential equations for N and \bar{R} , applicable to both isothermal and non-isothermal conditions, can be expressed by

$$\frac{dN}{dt} = \frac{g_1 - g_1 f_2 + g_3 f_1}{1 - f_2 - g_2 g_3 f_3}, \quad \frac{d\bar{R}}{dt} = \frac{f_1 - f_1 g_2 + f_3 g_1}{1 - g_2 - f_2 f_3 g_3}, \quad (15)$$

where the functions g_1, g_2, g_3 and f_1, f_2, f_3 are

$$g_1 = J + \frac{b\ell N}{x(\bar{R} - R_c)} \left(\frac{1}{T} - \frac{1}{x} \frac{d \ln C_\infty}{dT} \right) \frac{dT}{dt}, \quad (16)$$

$$g_2 = \frac{-N\bar{R}}{3(\bar{R} - R_c)} \Gamma, \quad g_3 = \frac{-N^2}{(\bar{R} - R_c)} \Gamma, \quad (17)$$

$$f_1 = \frac{D}{\bar{R}} \left(\frac{e^x C_\infty - C_{\bar{R}}}{C_p - C_{\bar{R}}} \right) + \frac{J}{N} (R_c + \delta R_c - \bar{R}) + \frac{b\ell}{x} \left(\frac{1}{x} \frac{d \ln C_\infty}{dT} - \frac{1}{T} \right) \frac{dT}{dt}, \quad (18)$$

$$f_2 = N\Gamma, \quad f_3 = \frac{\bar{R}}{3}\Gamma, \quad \Gamma = \frac{4\pi b\ell \bar{R}^2 (C_p - C_0)}{C_\infty e^x x^2 (1 - \frac{4\pi \bar{R}^3}{3} N)^2}. \quad (19)$$

In the above expressions, δR_c is the width of the size distribution and $b = 0.317014$ for $\bar{R} \leq 3R_c/2$ and $b = 0$ otherwise [4]. In computations, we assume $\delta R_c = a\ell$ with a , a positive constant $a < 1$, taken as a free parameter. It is noted

that the particular value of b set by Langer and Schwartz reproduces the familiar Lifshitz-Slyozov coarsening law “ $t^{1/3}$ ” as $t \rightarrow \infty$ [4, 13]. The initial conditions for the equations in (15) are

$$N(t = t_o) = N_o, \quad (20)$$

$$\bar{R}(t = t_o) = R_c + \delta R_c = \frac{\ell}{x} + a\ell, \quad (21)$$

where the starting time t_o is determined from $N_o = \int_0^{t_o} J(\tau)d\tau$; and N_o defines the lowest particle density of practical interest, here treated as a model parameter.

2. Numerical Method

The nonlinear ordinary differential equations (15) need to be evaluated numerically. In evaluations of the right-hand-side expressions of equations in (15), we make use of correlations for the solubility limit C_∞ and the diffusivity D , which are temperature-dependent material properties. We have used the MATLAB programming environment to solve these differential equations; more specifically the MATLAB solver ODE15S [14]. This is a variable order solver, which is intended to solve stiff systems of ordinary differential equations. The solver is invoked at each time step of the time-temperature history, and the evolution of N and \bar{R} during the time step is computed with ODE15S for each mesh point, based on the local temperature at beginning and end of the time step. In the solution procedure, the temperature is assumed to vary linearly with time during the time step.

III. APPLICATION

A. Isothermal experiment

The methods outlined in the foregoing section have been verified [15] against a number of measurements made in isothermal conditions for binary precipitates such γ' -Ni₃Al in Ni-14 at.%Al and Co in Cu-Co alloys [5, 16, 17, 18]. Here, we only report the results of our computations for cobalt precipitates in Cu-2.7 at.%Co alloy, for which isothermal annealing tests (at 823 K) were carried out by Wendth and Haasen [17]. The considered experiment involved measurements of the SPP number density as a function of annealing time and also the time variation of precipitate mean size was determined. These properties were measured by transmission electron microscopy (TEM) and atom probe field ion microscopy.

In order to simulate this test, we used the solubility limit for cobalt in copper proposed by Servi and Turnbull [19] $C_\infty = 712.85 \times 10^{-2875/T}$, where T is the absolute temperature and C_∞ is in atomic percent. For the diffusivity of cobalt in copper, we used the correlation by Döhl *et al.* [20], $D = 4.3 \times 10^{-5} e^{-25738/T}$, where D is in m^2s^{-1} . The matrix/SPP interface energy σ was in our analyses set to 0.22 Jm^{-2} , following the evaluation of data by Stowell [21]. The second phase particles in these alloys are of pure cobalt, which means that C_p is 100 at%. Both the particles and the matrix have a face-centered cubic (fcc) crystal structure. Moreover, the molar volume v_m of cobalt is $6.7 \times 10^{-6} \text{ m}^3\text{mole}^{-1}$. In analyses, we have set the model parameter N_o in Eq. (20) to $1 \times 10^{10} \text{ m}^{-3}$ and a in Eq. (21) to unity.

The calculated evolution of SPP number densities are compared with data in Fig. 2. The results are shown for two cases: For the nominal case, the nucleation rate J , given by Eq. (11), has been used. For the scaled case, the coefficient \mathcal{B} in Eq. (11) has been scaled by a factor 0.05, in order to obtain a best fit to the data. For this test at 823 K, shown in Fig. 2, the measured SPP density reaches a peak at about 300 seconds, after which coarsening starts to dominate the picture. At this stage, large particles will grow at the expense of smaller ones, as a consequence of the Gibbs-Thomson relation, see section IIB1. The smallest particles will ultimately dissolve, which makes the number density decrease with a rate proportional to $\approx 1/t$. Our model captures this behavior fairly well, but the calculated peak in the SPP density is reached too early, in comparison with data. For Cu-1.0 at.%Co alloy, LeGoues and Aaronson [16] reported a delay time of about 130 s in their study, whereas Haasen and Piller [18] reported that the delay time was no more than 30 s in the study made by Al-Kasab. Since we have utilized a steady-state theory and assumed a homogeneous nucleation rate, we could have overlooked the effect of the delay time, t_d , and hence get a discrepancy between the observed temporal data and calculated values; cf. Appendix C for a rough estimation of this effect.

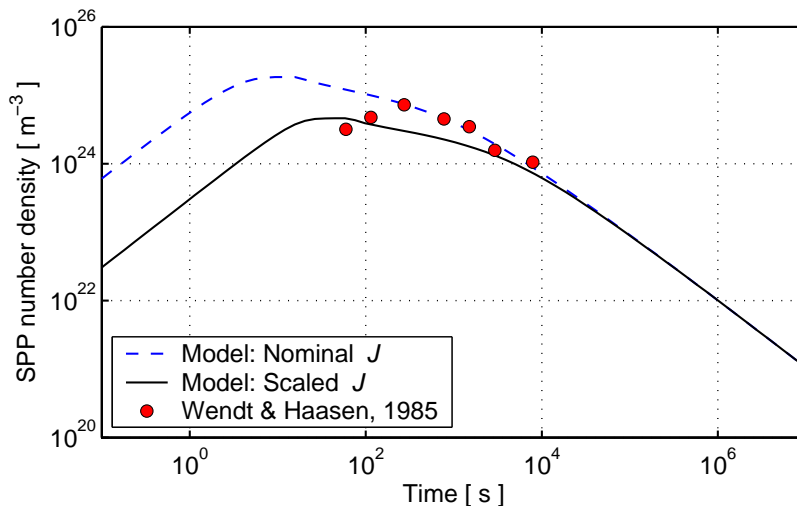


FIG. 2: Calculated number density of Co second phase particles in Cu-2.7at%Co at 823 K, in comparison with data from [17]. The calculated nucleation rate, given by Eq. (11), is scaled by a factor 0.05 in order to fit the data.

B. Non-isothermal simulation

In this subsection, we present the results of a simulation of a heat treatment made on a cylindrical specimen. The cylinder is made of Zircaloy-2 (Zr-1.4Sn-0.12Fe-0.09Cr by wt.%) and has a diameter of 25 mm. The heat treatment consists of quenching the sample from a high temperature (1323 K) body-centered cubic β phase in water, which is kept at room temperature. After the quenching, the cylinder is subjected to two subsequent annealing steps in Ar gas at 838 K (hexagonal-closed packed α phase) for durations of 1.0 h and 1.5 h, respectively (Fig. 3). The prominent

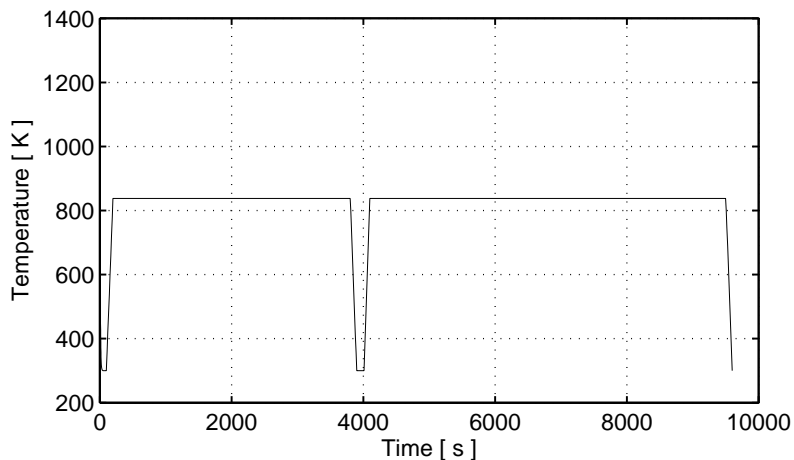


FIG. 3: Temperature history for the annealing steps; the cooling and heating rates for the steps are $\pm 5.4 \text{ K s}^{-1}$.

second phase precipitate in Zircalloys is $\text{Zr}(\text{Fe},\text{Cr})_2$ (Laves phase with hexagonal structure) formed at around 1200 K [22]. Here, we calculate the nucleation and growth of this kind of precipitates under the aforementioned heat treatment (quenching plus annealing) using the models described in the foregoing section, which are implemented in a computer program [23]. In particular, we have selected the nucleation rate equation (11) in our evaluation. Since

the diffusivity of Fe and Cr are similar and solubility data (temperature vs. concentration) are available for (Fe+Cr) in Zircaloy [22], we have treated the precipitate as a binary compound Zr and (Fe+Cr) with initial solute (Fe+Cr) concentration of $C_0 = 2010$ wppm (weight parts per million). The SPP molar volume is $v_m = 9 \times 10^{-6} \text{ m}^3 \text{ mole}^{-1}$ and its composition $C_p = 5.4 \times 10^5$ wppm. We have assumed that the diffusivity during nucleation is identical to that during growth. The input model parameters in our evaluations are as follows. We set the effective diffusivity for (Fe+Cr) in Zircaloy as $D(T) = 1.473 \times 10^{-6} e^{-15930/T}$, where T is the absolute temperature and D is in $\text{m}^2 \text{ s}^{-1}$, and the surface tension of the precipitate $\sigma = 0.25 \text{ Jm}^{-2}$. The lower cut-off limit for the particle density, N_o in Eq. (20), is set to $1 \times 10^{10} \text{ m}^{-3}$, and the model parameter a in Eq. (21) to 0.25. The motivations for selecting these values are discussed in [15].

The results of our non-isothermal evaluation are presented in a number of diagrams in Fig. 4, which shows (i) the mean precipitate radius, (ii) the precipitate number density, (iii) nucleation rate, (iv) the matrix supersaturation, (v) the matrix solute concentration (Fe+Cr), and (vi) temperature evolution in the first ten seconds of the heat treatment. The computation output corresponds to the center of the cylinder and 0.1 mm from the outer surface. The cooling rates at these locations, during quenching, can be noted from the temperature vs. time diagram in Fig. 4.

C. Discussion

From the results displayed in Fig. 4, we note that there is a significant difference in calculated precipitate radius at the different positions in the cylinder, directly upon β quenching, but this difference gradually diminishes under subsequent annealing. The initial difference in the radius of the precipitates located in the cylinder central region and those close to the outer surface follows from the difference in the cooling rate, as is seen in the temperature diagram in Fig. 4. According to our computations, the slow cooling at the cylinder central part results in appreciable precipitate growth already under the quenching phase. This behavior is not predicted at the billet outer surface.

The calculated time variation of the precipitate number density shown in Fig. 4 displays a remarkable difference between the central and periphery of the cylinder directly on quenching. The calculated number density at the outer surface is initially about several orders of magnitude larger than that at the central part, but this large difference gradually disappears under subsequent annealing as a result of coarsening. Figure 4 also shows the calculated nucleation rate as a function of time, evaluated at the considered locations in the cylinder. As can be seen, the nucleation takes place under a very short time span, as the temperature drops below 1118 K and the matrix becomes supersaturated ($C > C_\infty$). The nucleation rate pulse width, as can be seen in the diagram, is a couple of ms at the billet outer surface, whereas the corresponding time span is much larger in the central part, i.e., around 50 ms. The calculated matrix supersaturation, $x = \ln(C/C_\infty)$, is also shown as a function of time in the figure. The spikes seen in the diagram for x correspond to the temperature drops during the annealing cycles (Fig. 3), which reduce C_∞ . Note also the sharp dive in the matrix solute concentration due the temperature dip. The results of the computations presented here, i.e., the precipitate radius and number density, are in qualitative agreement with the observations made on a similar kind of heat treatment of this material [24].

As alluded in section III A, we have supposed a steady-state nucleation model. Such a treatment does not provide information regarding instantaneous SPP size distribution nor on the nucleation rate prior to reaching steady state. Some workers postulate a nucleation relation in the form $J(t) = J(\infty) \exp(-t_d/t)$ to fit metallurgical data [1]. However, this type of approach is simplistic and a more rigorous treatment to solve the time-dependent Fokker-Plank equation (3) [25] or extend the field theoretical approach (section III A) to the realm of phase transition dynamics can be more expedient. Besides, nucleation does not commonly occur homogeneously in a matrix by means of solely thermal and concentration fluctuations. It is induced most often by heterogeneities and defects in solids, e.g., grain and interphase boundaries, dislocations, stacking faults, free surfaces and vacancies or their clusters. These micro-domains facilitate or enhance the nucleation rate for formation of a new phase during quenching [26].

IV. CONCLUSION

The equations for nucleation, growth and coarsening of second phase precipitates are extended to account for the non-isothermal situations. The results of our simulation of the heat treatment of a Zircaloy-2 specimen clearly illustrates the influence of cooling rate during quenching on the properties of SPPs. A lower cooling rate results in larger precipitates with a smaller number density. This calculation is in qualitative agreement with the observations made on a similar kind of heat treatment of this material [24], which also indicate that SPP size and density are quenching rate dependent and they impact macroscopic properties of the alloy.

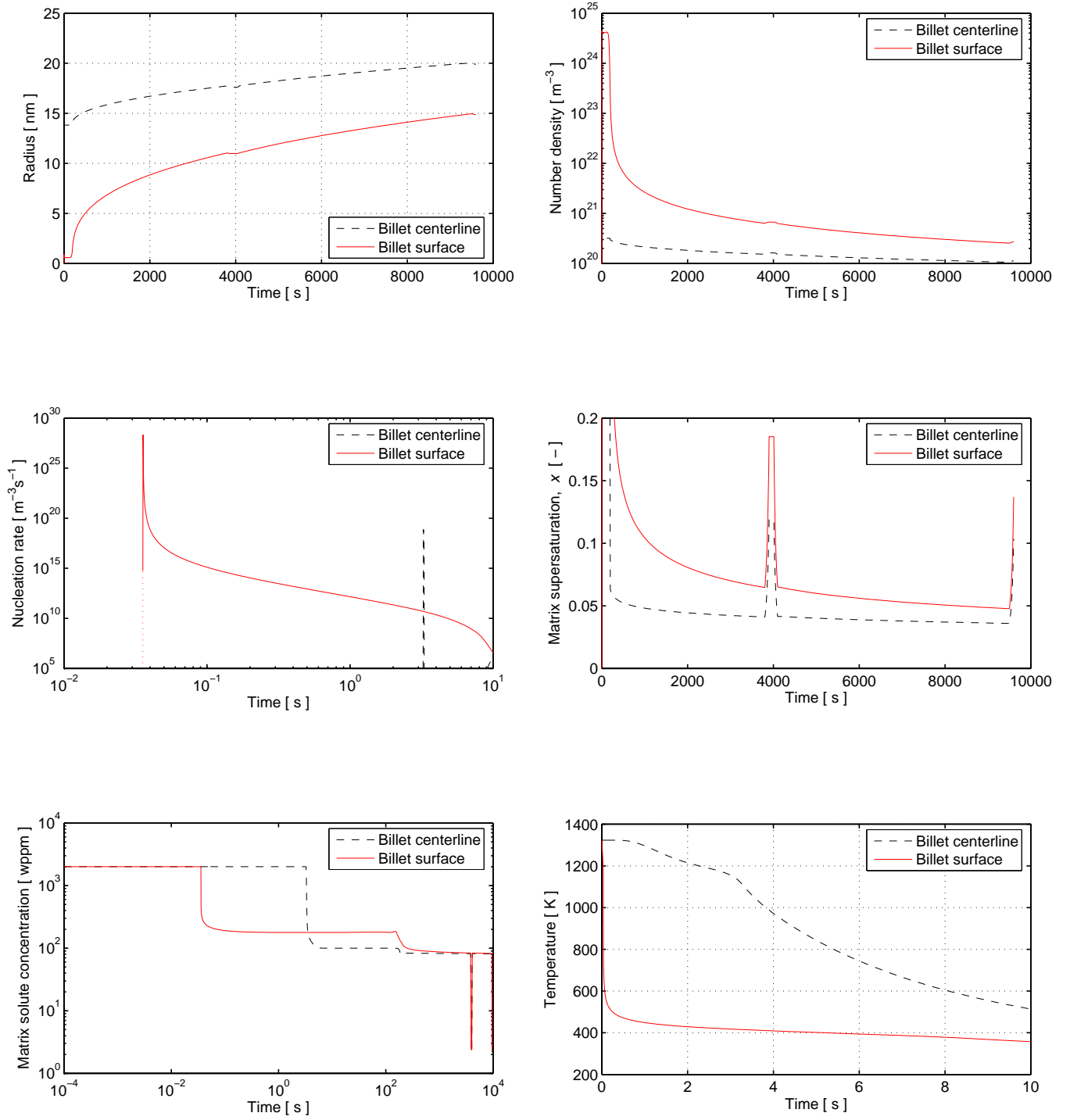


FIG. 4: Evolution of $\text{Zr}(\text{Fe,Cr})_2$ SPPs in a Zircaloy-2 cylinder during the heat treatment. Diagrams, left to right, top to bottom, show calculated (i) mean precipitate radius, (ii) precipitate number density, (iii) nucleation rate, (iv) matrix supersaturation, (v) matrix solute concentration (Fe+Cr), and (vi) temperature in the first ten seconds.

APPENDIX A: NUCLEATION RATE CLOSE TO THE CRITICAL DROPLET RADIUS

When the droplet (precipitate) radius R is close to its critical value R_c , the free energy, $F(R)$ in Eq. (1) can be approximated by, $F(R) = F_c - 0.5(d-1)S_d\sigma R_c^{d-3}(\delta R)^2$, with $\delta R = R - R_c$ [8]. The integrand in Eq. (4) is sharply peaked at R_c , thus the steepest descent method is used to evaluate the integral, resulting:

$$J = (2\pi)^{-1/2} B_c \left(\beta |F''(R_c)| \right)^{1/2} n_s(R_c), \quad (\text{A1})$$

Substituting $n_s(R_c) = n_l \exp[-\beta F(R_c)]$ and simplifying

$$J = (2\pi)^{-1/2} \Omega_c \varepsilon R_c n_l \exp(-\beta F_c). \quad (\text{A2})$$

Here, $\Omega_c = B_c \beta |F''(R_c)|$ is the nucleation frequency, $B_c = B(R_c)$ the critical kinetic coefficient for nucleation and $\varepsilon = (\beta |F''(R_c)| R_c^2)^{-1/2}$ with $F''(R_c) = (\partial^2 F / \partial R^2)_{R=R_c}$. Utilizing Eq. (1), we write, $\Omega_c = S_d B_c \beta \sigma (d-1) R_c^{d-3}$ and $\varepsilon^{-2} = S_d \beta \sigma (d-1) R_c^{d-1}$. Placing these last two relations into Eq. (A2), we obtain Eq. (5) of the main text.

APPENDIX B: STATISTICAL DESCRIPTION OF NUCLEATION RATE

The starting point for the statistical mechanics approach to nucleation theory is the Ginsburg-Landau free energy functional for a scalar field variable $\psi(\vec{r})$:

$$\tilde{F}(\psi) = \int d\vec{r} \left[\frac{K}{2} (\nabla\psi)^2 + U(\psi) \right], \quad (\text{B1})$$

where $\psi = \psi(\vec{r})$ is the order parameter, e.g., for a binary alloy it is the local concentration, K is a phenomenological constant designating the amplitude of the spatial gradient of ψ and U is the potential energy, which for a “ ψ^4 ” field theory is $U(\psi) = -\frac{r_0}{2}\psi^2 + \frac{u_0}{4}\psi^4 - h\psi$. Here the coefficients r_0 and u_0 are, in general, functions of pressure and temperature and h is an acting external field, which for the case of binary alloys is equivalent to the chemical potential. The potential U has two minima, $\psi_{\pm}(h)$. For $h > 0$, ψ_+ expresses the stable phase and ψ_- the metastable phase, whereas for $h < 0$ the roles of ψ_+ and ψ_- are reversed (Fig. 5).

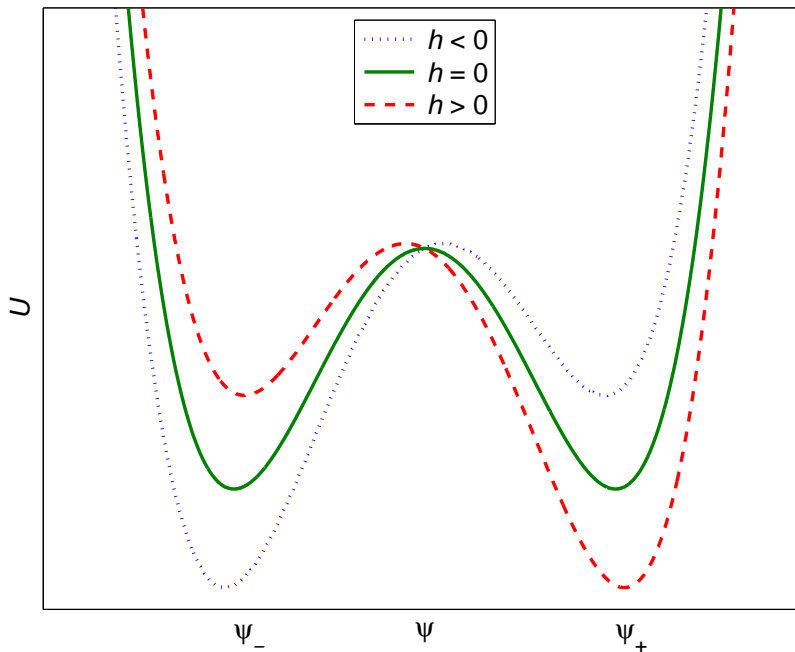


FIG. 5: The potential energy U with stable and metastable minima.

To proceed, consider the grand-canonical partition function for the system, defined as:

$$Z(h) = \int \delta\psi e^{-\beta\tilde{F}(\psi)}. \quad (\text{B2})$$

The extrema of the integrand in Z are the solutions of the equilibrium equation, i.e.,

$$K\nabla^2\psi + r_0\psi - u_0\psi^3 + h = 0. \quad (\text{B3})$$

One solution of interest, for small h , is the saddle point solution, $\bar{\psi}$. It describes a radially symmetric particle of the nucleating phase embedded in a spatially uniform metastable background. Its profile is approximated by

$$\bar{\psi} \approx \frac{1}{2}(\psi_+ + \psi_-) + \frac{1}{2}(\psi_+ - \psi_-) \tanh \left[\frac{r - R}{\sqrt{2}\xi} \right], \quad (\text{B4})$$

where $\psi(r=0) = \psi_-$ and $\psi(r \rightarrow \infty) = \psi_+$ are the stable and metastable values of the order parameter, corresponding to the two minima of $U(\psi)$, describing a stable particle in a metastable surrounding, r is the radial position, R the particle radius and $\xi = (K/2r_0)^{1/2}$ is the interface thickness called the correlation length. In a ψ^4 field theory the correlation length is related to the capillary length ℓ , cf. section II A, according to $\xi = 6\ell$ [8].

The free energy $\tilde{F}(\psi)$ may be expanded around the saddle point $\bar{\psi}$. Using Dirac's concise notation, we write

$$\tilde{F}(\psi) = \bar{F} + \frac{1}{2}\langle u|\mathcal{M}|u\rangle + \mathcal{O}(u^3), \quad (\text{B5})$$

where $\bar{F} = F(\bar{\psi})$, $u = \psi - \bar{\psi}$, and $\mathcal{M} = -K\nabla^2 - U''(\bar{\psi})$. We note that since $\bar{\psi}$ is a saddle point there is one negative eigenvalue which reflects the instability of the critical particle. Moreover, there are d zero eigenvalues associated with the translational modes of the particle in d -dimension. More explicitly, as Langer [27] showed, the eigenvalues in the second order in h can be expressed by

$$\lambda_{0l} = \frac{(l-1)(l+d-1)}{R_c^2} \left[1 + \mathcal{O}\left(\frac{l^2\xi^2}{R_c^2}\right) \right], \quad l = 0, 1, 2, \dots \quad (\text{B6})$$

where $R_c = (d-1)\sqrt{2Kr_0}/(3h\sqrt{u_0})$ is the critical radius of the nucleus. Here, λ_{00} is the only negative eigenvalue, whereas λ_{01} is the d -fold degenerate zero eigenvalue. The energy of the lowest mode $l=0$ is negative, implying that in the context of a steepest descent calculation the critical particle generates the imaginary part of the free energy in the metastable state.

As it has been pointed out in [10], in the case of interest ($h \rightarrow 0$, $R_c \rightarrow \infty$), the eigenfunctions of \mathcal{M} form a band of soft modes which describe the surface excitations of the spherical critical particle. In fact, the eigenfunction corresponding to $l=1$ is the Goldstone mode associating with the spontaneous breaking of translational invariance by the center of the droplet. Apart from the unstable and translational modes the remaining eigenvalues of \mathcal{M} , λ_{nl} are positive describing stable distortion of the critical spherical particle [27].

To calculate the nucleation rate, we first express the partition function (B2) in the form of the linked-cluster expansion, viz.,

$$Z = Z_0 \exp\left(\frac{Z_1}{Z_0}\right), \quad (\text{B7})$$

where Z_0 represents the contribution from the metastable minimum and Z_1 that from the path $\bar{\psi}$. The contribution from the metastable minimum $Z_0 = \exp[-\beta F(\psi)]$, with $\psi(r) = \hat{\psi}_+ + \eta(r)$ is written in the form

$$Z_0 = \exp[-\beta F(\hat{\psi}_+)] \prod_j \left(\frac{\pi}{\beta R^d \lambda_j^{(0)}} \right)^{1/2}, \quad (\text{B8})$$

where $\lambda_j^{(0)}$ are the eigenvalues of the equation: $\mathcal{M}_0 \eta_j^{(0)} = \lambda_j^{(0)} \eta_j^{(0)}$ with $\mathcal{M}_0 = -K\nabla^2 - r_0/2 + 1.5u_0\hat{\psi}_+^2$. Here $\hat{\psi}_+ = 2(r_0/3u_0)^{1/2} \cos\theta$ where $3\theta = \arccos[1.5h(3u_0/r_0^3)^{1/2}]$ is the stable solution of Eq. (B3) for $\nabla^2\psi = 0$ and $h > 0$. The saddle point contribution to the partition function can be written as

$$Z_1 = \exp[-\beta F(\bar{\psi})] \mathcal{J} \mathcal{V} \prod'_{n,l} \left(\frac{\pi}{\beta R^d \lambda_{nl}} \right)^{(2l+1)/2}, \quad (\text{B9})$$

where the prime denotes that the zero modes are removed and \mathcal{J} is the Jacobian that arises in integration and \mathcal{V} denotes the contribution of zero modes and is proportional to the system volume V . The free energy of the system is $\mathcal{F} = \lim_{V \rightarrow \infty} \beta^{-1} V^{-1} \ln Z$. Writing Eq. (B7) in the form $\ln Z = \ln Z_0 + Z_1/Z_0$ and using Eqs. (B8) and (B9), the droplet free energy is expressed by

$$\mathcal{F} = \exp[-\beta F(\bar{\psi})] \mathcal{J} \mathcal{V} r_0^{d/2} \exp \left[\sum_{l \neq 1}^L \ln \left(\frac{r_0}{\lambda_{0l}} \right)^{\nu_l/2} \right], \quad (\text{B10})$$

where ν_l is the degeneracy of the d -dimensional spherical harmonics, e.g., for $d = 2$, $\nu_l = 2$ while for $d = 3$, $\nu_l = 2l + 1$. The upper limit of the sum L is given by $L \sim R_c^2 r_0$, for which the approximation (B6) becomes invalid. Günther, Nicole and Wallace [10] have calculated the factors in Eq. (B10). Placing $\rho \equiv r_0^{3/2}/(|h|\sqrt{u_0})$, these factors are

$$F(\bar{\psi}) = c \frac{r_0^{(4-d)/2}}{u_0} \rho^{d-1}, \quad (\text{B11})$$

$$\mathcal{J} = \rho^{(d-1)d/2} r_0^{(4-d)d/4} u_0^{-d/2}, \quad (\text{B12})$$

and the spectrum of excitations are calculated to be

$$\exp \left[\sum_{l \neq 1}^L \ln \left(\frac{r_0}{\lambda_{0l}} \right)^{\nu_l/2} \right] \propto \begin{cases} i \rho^{-d} \exp(k_0 \rho^{d-1}) & d \neq 3 \\ i \rho^{-2/3} \exp(k_0 \rho^2) & d = 3 \end{cases} \quad (\text{B13})$$

where c and k_0 are dimensionless constants and $i = \sqrt{-1}$. The nucleation rate à la Langer [9] is $J = \beta \kappa \Im(\mathcal{F})/\pi$ with κ being a kinetic factor; Eqs. (B11), (B12) and (B13) can be assembled according to Eq. (B10) to yield the GNW relation [10] in the regime of interest ($h \rightarrow 0$, $R_c \rightarrow \infty$), viz.,

$$\lim_{h \rightarrow 0} J = \begin{cases} A \kappa r_0^{d/2} \left(\frac{r_0^{(4-d)/2}}{u_0} \right)^{d/2} \rho^{d(d-3)/2} \exp \left[-\frac{r_0^{(4-d)/2}}{u_0} (c \rho^{d-1} + \dots) \right] & d \neq 3 \\ A \kappa r_0^{3/2} \left(\frac{r_0^{1/2}}{u_0} \right)^{3/2} \rho^{7/3} \exp \left[-\frac{r_0^{1/2}}{u_0} (c \rho^2 + \dots) \right] & d = 3 \end{cases} \quad (\text{B14})$$

Now by transcribing the ψ^4 -theory parameters to the pertinent variables in alloys, we identify $\alpha_d^{1/(d-1)} \rho \Leftrightarrow (x_0/x)$, where $\alpha_d \equiv r_0^{(4-d)/2}/u_0$ is an auxiliary variable and the variables x and x_0 are defined in section IIA. Setting $\xi = r_0^{-1/2}$ (with $K = 2$), we convert Eq. (B14) to

$$J \sim \begin{cases} \alpha_d^{d/(d-1)} \kappa \xi^{-d} \left(\frac{x_0}{x} \right)^{d(d-3)/2} \exp \left[-\left(\frac{x_0}{x} \right)^{d-1} \right] & d \neq 3 \\ \alpha_3^{1/3} \kappa \xi^{-3} \left(\frac{x_0}{x} \right)^{7/3} \exp \left[-\left(\frac{x_0}{x} \right)^2 \right] & d = 3 \end{cases} \quad (\text{B15})$$

From here on, to obtain Eq. (10) is fairly straightforward, as it has been explicitly shown by Langer and Schwartz [4].

APPENDIX C: NUCLEATION DELAY TIME

In order to calculate the time-lag for nucleation in classical theory, one needs to solve the full Fokker-Planck equation (3). Here, however, we can make a rough estimate of this quantity for the case of $t \gg B^{-1}$, meaning that; we are interested in time intervals much larger than the time of relaxation ($\propto B^{-1}$). We assume that $n = n(R, t)$ obeys:

$$\frac{\partial n}{\partial t} = B(R_c) \frac{\partial^2 n}{\partial R^2}, \quad (\text{C1})$$

subject to the boundary conditions $n(0, t) = n_1$, $n(s, t) = 0$ and the initial condition $n(R, 0) = 0$ for $s \geq R_c$. The solution of this boundary value problem is expressed as

$$n(R, t) = n_1 \left(1 - \frac{R}{s} \right) - \frac{2n_1}{\pi} \sum_{m=1}^{\infty} \frac{1}{m} \sin \left(\frac{m\pi R}{s} \right) e^{-\frac{m^2 \pi^2 B_c t}{s^2}}. \quad (\text{C2})$$

The nucleation rate is related to the gradient of $n(R, t)$, viz.,

$$J(s, t) \approx -B_c \left. \frac{\partial n}{\partial R} \right|_{R=s} = \frac{B_c n_1}{s} \vartheta_4(0, q), \quad (\text{C3})$$

where $\vartheta_4(u, q) = 1 + 2 \sum_{m=1}^{\infty} (-1)^m q^{m^2} \cos(2mu)$ is an elliptic theta function [28], here with $q \equiv \exp(-B_c \pi^2 t/s^2)$. Employing the Courant-Hilbert identity [29],

$$\sum_{m=-\infty}^{\infty} \exp(-\pi m^2 \zeta) (-1)^m = \frac{1}{\sqrt{\zeta}} \sum_{m=-\infty}^{\infty} \exp\left[-\frac{\pi(m-1/2)^2}{\zeta}\right], \quad (\text{C4})$$

Eq. (C3) can be expressed in the form

$$J(s, t) = \frac{B_c n_1}{\sqrt{\pi s}} \left(\frac{t_d}{t}\right)^{1/2} \vartheta_2(0, e^{-\frac{t_d}{t}}), \quad (\text{C5})$$

where $t_d \equiv s^2/B_c$ is the delay time. For short times, $t \ll t_d$, power series expansion of the theta function gives

$$J(s, t) \sim \frac{2B_c n_1}{\sqrt{\pi s}} \left(\frac{t_d}{t}\right)^{1/2} \left[e^{-\frac{t_d}{t}} + \mathcal{O}\left(e^{-\frac{9t_d}{4t}}\right)\right]. \quad (\text{C6})$$

Equation (C5) offers a zeroth approximation to the time-dependence of the nucleation rate, however, it illustrates the essential physics of the phenomenon. Detailed calculations of the time-dependent nucleation rate and the delay time, within the classical nucleation theory, can be found in Refs. [30, 31].

-
- [1] R. Wagner and R. Kampmann, in *Phase Transformation in Materials*, edited by P. H. R.W. Cahn and E. Kramer (VCH, Weinheim, Germany, 1991), vol. 5 of *Material Science and Technology*, chap. 4.
- [2] J. D. Gunton, M. S. Miguel, and P. S. Sahni, in *Phase Transitions in Critical Phenomena*, edited by C. Domb and J. L. Lebowitz (Academic Press, London, England, 1983), vol. 8, chap. 3, pp. 267–479.
- [3] K. Binder, in *Phase Transformation in Materials*, edited by P. H. R.W. Cahn and E. Kramer (VCH, Weinheim, Germany, 1991), vol. 5 of *Material Science and Technology*, chap. 7.
- [4] J. S. Langer and A. J. Schwartz, *Physical Review A* **21**, 948 (1980).
- [5] H. Wendt and P. Haasen, *Acta Metallurgica* **31**, 1649 (1983).
- [6] R. Kampmann and R. Wagner, in *Decomposition of Alloys: in the early stages*, edited by P. Haasen, V. Gerold, R. Wagner, and M. Ashby (Pergamon Press, Oxford, England, 1984), pp. 91–103.
- [7] E. M. Lifshitz and L. P. Pitaevskii, *Physical Kinetics* (Pergamon Press, Oxford, England, 1981), chap XII.
- [8] A. Onuki, *Phase Transition Dynamics* (Cambridge University Press, Cambridge, UK, 2002).
- [9] J. S. Langer, *Annals of Physics* **54**, 258 (1969).
- [10] N. J. Günther, D. A. Nicole, and D. J. Wallace, *Journal of Physics A: Mathematical and General* **13**, 1755 (1980).
- [11] H. I. Aaronson and F. K. LeGoues, *Metallurgical Transactions A* **23A**, 1915 (1992).
- [12] L. Ratke and P. W. Voorhees, *Growth and Coarsening - Ripening in Material Processing* (Springer-Verlag, 2002).
- [13] I. M. Lifshitz and V. V. Slyozov, *Journal of Physics and Chemistry of Solids* **19**, 35 (1961).
- [14] The MathWorks Inc., *Using MATLAB Version 6* (Natick (MA), U.S.A., 2000).
- [15] L. O. Jernkvist, Tech. Rep. TR 05-002, Quantum Technologies AB, Uppsala, Sweden (2005).
- [16] F. K. LeGoues and H. I. Aaronson, *Acta Metallurgica* **32**, 1855 (1984).
- [17] H. Wendt and P. Haasen, *Scripta Metallurgica* **19**, 1053 (1985).
- [18] P. Haasen and J. Piller, *Zeitschrift für Metallkunde* **78**, 757 (1987), (In German).
- [19] I. S. Servi and D. Turnbull, *Acta Metallurgica* **14**, 161 (1966).
- [20] R. Döhl, M. P. Macht, and V. Naundorf, *Physica Status Solidi A* **86**, 603 (1984).
- [21] M. J. Stowell, *Materials Science and Technology* **18**, 139 (2002).
- [22] A. R. Massih, T. Andersson, P. Witt, M. Dahlbäck, and M. Limbäck, *Journal of Nuclear Materials* **322**, 138 (2003).
- [23] L. O. Jernkvist and A. R. Massih, Tech. Rep. TR 04-007, Quantum Technologies, Uppsala, Sweden (2005).
- [24] A. R. Massih, M. Dahlbäck, M. Limbäck, T. Andersson, and B. Lehtinen, *Corrosion Science* (2005), (In press).
- [25] D. Kashchiev, *Nucleation, Basic Theory with Applications* (Butterworth, Heinemann, Oxford, UK, 1999).
- [26] D. Porter and K. Easterling, *Phase Transformations in Metals and Alloys* (Chapman & Hall, London, UK, 1992).
- [27] J. S. Langer, *Annals of Physics* **41**, 108 (1967).
- [28] E. T. Whittaker and G. N. Watson, *A Course of Modern Analysis* (Cambridge University Press, Cambridge, UK, 1927).
- [29] R. Courant and D. Hilbert, *Methods of Mathematical Physics* (Wiley, New York, USA, 1966), see vol. 2, page 200.
- [30] K. Binder and D. Stauffer, *Advances in Physics* **75**, 343 (1976).
- [31] D. Kashchiev, *Surface Science* **14**, 209 (1969).